Journal of Medicinal Chemistry

Article

pubs.acs.org/jmc

KDM4B as a Target for Prostate Cancer: Structural Analysis and Selective Inhibition by a Novel Inhibitor

Chia-Han Chu,[†,‡,#] Ling-Yu Wang,[§,#] Kai-Cheng Hsu,[∥,#] Chung-Chin Chen,[†] Hsing-Hung Cheng,[†] Szu-Min Wang,[†] Chien-Ming Wu,[†] Tsan-Jan Chen,[†] Ling-Ting Li,[∥] Ruiwu Liu,[§] Chiu-Lien Hung,[§] Jing-Moon Yang,*[,∥] Hsing-Jien Kung,*[,§,⊥] and Wen-Ching Wang*[,†,‡]

[†]Institute of Molecular and Cellular Biology and Department of Life Sciences and [‡]Biomedical Science and Engineering Center, National Tsing-Hua University, Hsinchu, 30013, Taiwan

[§]Department of Biochemistry and Molecular Medicine, University of California Davis School of Medicine, University of California Davis Cancer Center, Sacramento, California 95817, United States

[∥]Institute of Bioinformatics and Systems Biology, National Chiao Tung University, Hsinchu, 30050, Taiwan

[⊥]National Health Research Institutes, Miaoli, 35053, Taiwan

Supporting Information

ABSTRACT: The KDM4/JMJD2 Jumonji C-containing histone lysine demethylases (KDM4A–KDM4D), which selectively remove the methyl group(s) from tri/dimethylated lysine 9/36 of H3, modulate transcriptional activation and genome stability. The overexpression of KDM4A/KDM4B in prostate cancer and their association with androgen receptor suggest that KDM4A/KDM4B are potential progression factors for prostate cancer. Here, we report the crystal structure of the KDM4B·pyridine 2,4-dicarboxylic acid·H3K9me3 ternary complex, revealing the core active-site region and a selective K9/K36 site. A selective KDM4A/KDM4B inhibitor, **4**, that occupies three subsites in the binding pocket is identified by virtual screening. Pharmacological and genetic inhibition of KDM4A/KDM4B significantly blocks the viability of cultured prostate cancer cells, which is accompanied by increased H3K9me3 staining and transcriptional silencing of growth-related genes. Significantly, a substantial portion of differentially expressed genes are AR-responsive, consistent with the roles of KDM4s as critical AR activators. Our results point to KDM4 as a useful therapeutic target and identify a new inhibitor scaffold.

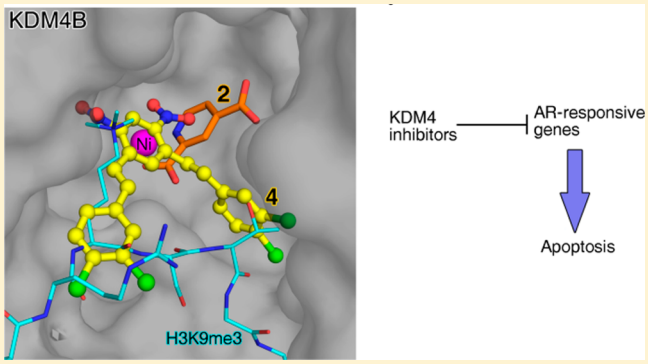

INTRODUCTION

Histone lysine demethylases (KDMs), which regulate a dynamic, reversible status of "methyl" histone codes, have gained much attention since the first discovery of KDM1/LSD1 in 2004.[1] Mutations, amplifications, deletions, and aberrant expression of KDMs have been identified in a variety of cancers, and their roles in modulating the behavior of cancer cells have been substantiated.[2] As such, increasing attention has been paid to evaluating KDMs as potential therapeutic targets for cancer.[3] There are now eight KDM families, including 28 members that have been identified (for a review, see ref 3b). KDM2–KDM8 constitute a large superfamily that shares a Jumonji C (JmjC) domain, which functions as an α-ketoglutarate (AKG) and Fe(II)-dependent demethylase. Notably, each family exhibits its exquisite substrate specificity toward different histone lysine residues, thereby effectively integrating upstream signals and modulating chromatin conformation.[1c]

Among these, the largest gene family, KDM4 (four paralogues, KDM4A–KDM4D, and two pseudogenes, KDM4E and KDM4F), has been shown to be an eraser of a repressive mark, H3K9me3/me2, whereas its subfamily, KDM4A–KDM4C, also demethylates H3K36me3/me2.[4] KDM4A and KDM4B are overexpressed in a variety of cancers including prostate, breast, colorectal, lung, gastric, esophageal, lymphoma, renal, and medulloblastoma.[4b] For prostate and breast cancers, this family of demethylases has the added significance of being coactivators of androgen receptor (AR) (KDM4A–KDM4D)[5] and estrogen receptor (ER) (KDM4A and KDM4B).[6] They function to stimulate the transcriptional potential of the receptors. KDM4B also regulates the turnover of AR.[5c] Given the important roles of AR and ER in prostate and breast carcinogenesis, KDM4A/KDM4B are considered to be promising drug targets for intervening in these malignancies.[3b,4b]

Thus far, the inhibitors described for KDM4 proteins are largely AKG analogues: *N*-oxalylglycines (OGAs), including OGA (**1**), which inhibits KDM4A, KDM4C, and KDM4D,[7]

Received: February 15, 2014
Published: June 27, 2014

   dx.doi.org/10.1021/jm500249n | J. Med. Chem. 2014, 57, 5975–5985

pyridine 2,4-dicarboxylic acids (PD2s) developed based on KDM4E,[8] and 8-hydroxyquinolines (8HQs), including **3** (8HQ).[9] Yet, as a prodrug, the cytotoxic IC_{50} of compound **2** (PD2) is in the millimolar range in cultured cells because of its poor cell-penetrating ability,[10] whereas 5-carboxy-8HQ, with a potent inhibitory effect on KDM4E in vitro (IC_{50} = 0.2 μM), exhibits a relatively high cytotoxic IC_{50} in HeLa cells (86.5 μM).[9] In this investigation, we determined the KDM4B·**2**·H3K9me3 ternary complex structure and applied a structure-guided strategy to identify a selective inhibitor, 1,5-bis[(*E*)-2-(3,4-dichlorophenyl)ethenyl]-2,4-dinitrobenzene (NSC636819), toward KDM4A and KDM4B. Kinetic analysis reveals that compound **4** (NSC636819) is a competitive inhibitor of KDM4A/KDM4B. Furthermore, we report that pharmacological and genetic inhibition of KDM4A/KDM4B significantly lowers the viability of prostate cancer cells, principally because of its potency toward inhibiting the AR transcriptional network.

MATERIALS AND METHODS

Cloning, Expression, and Purification. Human KDM4B (1−348) and KDM4A (1−347) were PCR-amplified from cDNAs using the following primers: KDM4B 1−348 forward, 5′-AAACATATGGGGTCTGAGGACCACGGCGCC-3′ (*Nde*I); KDM4B 1−348 reverse, 5′-AAAAAACTCGGGGCTCTCGAGCTACGTGGGCCG-3′ (*Xho*I); KDM4A 1−347 forward, 5′-AAACATATGGCGAGCGAAAGCGAAACTCTG-3′ (*Nde*I); and KDM4A reverse, 5′-AAAGGATCCCTACGTGGGCAGAGTATGGTC-3′ (*Bam*HI). The KDM4E catalytic domain (residues 1−347) was subcloned from pcDNA-KDM4E, a gift of Dr. Yoshihiro Izumiya (University of California Davis School of Medicine, Sacramento, CA), using the primers 5′-GGGGCTAGCATGAAGTCTGTGCACTC-3′ (*Nhe*I) and 5′-CCTCTCGAGCTAGGGCTCTGTGTGTTC-3′ (*Xho*I). PCR was performed with the HiFi DNA polymerase kit using a C1000 Touch thermal cycler (Bio-Rad Laboratories, Inc., USA). The amplified products were inserted into pET28a or pET30a (Novagen, Inc., USA) to generate pET28a-KDM4A(1−347), pET28a-KDM4B(1−348), and pET28a-KDM4E(1−347). The KDM4D construct containing the catalytic domain (residues 1−350) was a gift from Dr. Shi Yang (Harvard Medical School, Boston, MA). Expression of protein in *Escherichia coli* BL21 (DE3) was induced by addition of 0.5 mM isopropyl-β-D-thiogalactopyranoside (IPTG) at 16 °C for 21 h. The His6-tagged proteins were purified by a nickel affinity column (Ni Sepharose high performance, GE Healthcare). The protein was concentrated and further purified by a 16/60 Superdex 75 gel filtration column equilibrated with 50 mM HEPES, pH 7.5, and 500 mM NaCl. The protein purity was analyzed by SDS-PAGE. Protein concentration was assayed by the Bradford method using bovine serum albumin as the standard.[11]

Enzyme Assay. A formaldehyde dehydrogenase (FDH)-coupled demethylase assay was used to determine demethylase activity and to select potent inhibitors. All inhibitors were dissolved in dimethyl sulfoxide (DMSO) at various concentrations and added to the mixture such that the final DMSO concentration was 5%. The reagents for the demethylase reactions were dissolved in HEPES buffer (50 mM, pH 7.5), with the exception of Fe(II) solutions, which were made using $(NH4)_2Fe(SO_4)_2$ dissolved in 20 mM HCl to make a 400 mM stock solution. All reagents were stored at −30 °C. FDH, NAD+, TKQTARK$(Me)_3$STGGKAPR ($H3_{3-17}$K9me3), STGGVK-$(Me)_3$KPHRY ($H3_{31-41}$K36me3), or ARTK$(Me)_3$QTARK-$(Me)_2$STGGKAPRKQLATKA ($H3_{1-24}$K4me3K9me2) peptides (Kelowna Int. Sci. Inc.), DMSO, and the demethylase enzyme were added first to 96-well black immuno plate (SPL Life Science) and incubated together on ice for 15 min. Then, the plate was put into a FLUOStar OPTIMA ELISA reader (BMG LABTECH) at 37 °C, and the reaction was started by adding ascorbic acid (ascorbate), Fe(II), and AKG to final concentrations of 50 mM HEPES, pH 7.5, 2 μM of KDM4B, 5% DMSO, 0.01 U FDH (Sigma), 1 mM NAD+, 1 mM AKG, 2 mM ascorbate, 50 μM Fe(II), and various concentration of H3K9me3 peptide; the final volume was 50 μL. Each reaction was incubated at 37 °C for 30 min, and the production of NADH was detected by fluorescence (ex 360/em 470).

Crystallization. Crystallization was performed by the hanging-drop vapor-diffusion method at 4 °C. Equal volumes of a protein sample and the reservoir solution were mixed. Initial crystallization screening was automated using a Oryx8 robot (Douglas Instruments, UK) and the reagents of seven sets of crystallization kits: Crystal Screen I and II kits (Hampton Research), Index kit (Hampton Research), Clear Strategy Screen I and II kits (Molecular Dimension), Wizard kit (Emerald), and JB Screen classic HTS I and II kits (Jena Bioscience). Crystals of KDM4B (10 mg/mL protein, 4 mM compound **2** and 5 mM H3K9me3 peptide) were grown in 0.1 M MES (pH 6.5), 0.2 M magnesium acetate, and 20% (w/v) poly(ethylene glycol) (PEG) 8000. Optimized crystals used for diffraction (12 mg/mL within 4 mM **2** and 5 mM H3K9me3 peptide) were grown in 0.1 M MES (pH 6.5), 0.2 M magnesium acetate, 24% (w/v) PEG 8000. The crystal diffracted to 1.87 Å, belonged to space group *P*212121, and had unit cell dimensions of a = 54.36, b = 78.48, c = 83.89 Å. The asymmetric unit contained one molecule.

X-ray Data Collection and Processing. Crystals were flash-frozen in a stream of liquid nitrogen and then screened and characterized using an RU-300 rotating-anode X-ray generator (Rigaku/MSC Inc., USA) at the Macromolecular X-ray Crystallographic Laboratory of National Tsing Hua University, Taiwan. The KDM4B·**2**·H3K9me3 data set was collected at the SPring-8 BL12B2 beamline, Japan, with an ADSC Quantum 4R detector. All data sets were indexed, integrated, and scaled using HKL-2000.[12] Data collection statistics are shown in Table S2 of the Supporting Information.

Structure Determination and Refinement. Crystallographic refinement used the maximum-likelihood target function module in REFMAC5.[13] The KDM4B·**2**·H3K9me3 structures were constructed by MOLREP with KDM4A (PDB: 2YBS) as the template[13,14] and were refined using REFMAC5 coupled with ARP/wARP,[15] which automatically added water molecules. The $2F_o - F_c$ electron density maps were generated by FFT and plotted by PyMOL. The validities of the KDM4B·**2**·H3K9me3 structure were assessed by PROCHECK.[16]

Structural Comparison. The KDM4B structure was compared with protein structures in the DALI server (http://ekhidna.biocenter.helsinki.fi/dali_server/). The structures of KDM4A·$H3_{1-17}$K9me3 (PDB code: 2P5B),[17] KDM4B·**2** (PDB code: 4LXL; this study), KDM4C·**1** (OGA) (PDB code: 2XML), KDM4D·AKG·$H3_{6-15}$K9me3 (PDB code: 4HON),[18] and KDM4E·**2** (PDB code: 2W2I) were superimposed by LSQMAN in O.[19] ESPript was used for the combined sequence as well as for secondary structure alignments and figure preparation.[20] PyMol (http://www.pymol.org) was used to prepare the figures.

Virtual Screening. The binding site for virtual docking screening of putative inhibitors was prepared by including protein atoms located in a ≤10 Å radius sphere centered around the bound ligand of KDM4A (PDB code: 2YBK[21]). We utilized GEMDOCK[22] to screen the NCI database (236 962 compounds). Top ranked compounds available from the Developmental Therapeutics Program of the National Cancer Institute were selected for testing in the KDM4A/KDM4B inhibitory assay.

Cell Culture. Primary PrEC cells were purchased from Clonetics (Walkersville, MD) and cultured in serum-free prostate epithelial cell growth medium following the vendor's directions. Cell lines RWPE1, LNCaP (LNCaP-FGC), CWR22Rv1 (22Rv1), VCaP, DU145, PC3 (all purchased from ATCC), and PNT2 (Sigma-Aldrich, MO) were cultured under their recommended conditions. CWR-R1[23] and LNCaP derived C4-2 and C4-2B cells[24] were cultured in RPMI1640 medium containing 10% FBS.

RNA Interference and Quantitative RT-PCR. Lentiviral vector pLKO.1 carrying sequences encoding a shRNA that specifically targets KDM4A and KDM4B gene (TRC library clone nos. TRCN0000234910 and TRCN000018014) were cotransfected with

viral packaging plasmids in 293T cells to generate the shRNA lentiviral particles. Empty pLKO.1 plasmid was used as negative control. The lentiviral supernatant was collected 48 h after transfection and concentrated by Lenti-X Concentrator (Clontech, CA). The precipitated viral particles were resuspended in fresh RPMI1640 medium with 10% FBS for subsequent LNCaP infection and were transduced into LNCaP cells for 72 h. Cells were then harvested, and total RNA was isolated, followed by cDNA synthesis and real-time PCR analysis using iQ5 iCycler thermal cycler (Bio-Rad, CA). Threshold cycle values were normalized against actin transcript level. Individual samples were performed in triplicate and converted to relative gene expression using QGene96 software (http://www.gene-quantification.de/download.html#qgene). Primer sequences used are as follows: KDM4A-F, 5′-AGGAGAGTGAACTGCCTCCA-3′; KDM4A-R, 5′-GGTCTCCTTCCTCTCCATCC; KDM4B-F, 5′-TCACGCAGTACAATATCCAG-3′; KDM4B-R, 5′-TCGTCA-TCATACAAAGAGCC; actin-F, 5′-GTACCACTGGCATCGTGAT-GGACT-3′; and actin-R, 5′CCGCTCATTGCCAATGGTGAT-3′.

Cell Proliferation Assay. LNCaP cells were seeded in a 48-well plate 1 day prior to lentivirus infection. After being subjected to the shRNA lentivirus (day 0), cell proliferation was measured every 2 days by MTT colorimetric assay according to the manufacturer's instruction (Roche, IN).

Immunoblotting and Flow Cytometry. Total cell lysates were obtained by lysing the cells with buffer (50 mM Tris-HCl, pH7.5, 150 mM NaCl, 0.5% Triton X-100, 10% glycerol, 1 mM EDTA, protease inhibitors) for 15 min on ice, followed by 10 min of sonication cycling (30 s on, 30 s off) on ice. The level of total histone H3 and trimethylated histone H3 Lys9 was analyzed by western blotting using anti-histone H3 (Cell Signaling, 4499) and anti-H3K9me3 (Millipore, 61021) antibodies. Mock- and inhibitor-treated cells were harvested and fixed with 70% ethanol for >4 h at −20 °C, followed by propidium iodide (Sigma-Aldrich) staining. The DNA content was analyzed by Becton Dickinson FACScan flow cytometry, and the sub-G1 population was quantified by WinMDI 2.9.

Microarray. LNCaP cells treated with mock or inhibitor **4** for 3 days were harvested, and the total RNA was extracted using TRIzol reagent (Life Technologies, NY). Microarray analysis was performed by the University of California Davis Cancer Center Gene Expression Resource, using Affymetrix Human Genome U133A (HG-U133A) GeneChip arrays (Affymetrix, CA), which permits expression analysis of the entire Genbank RefSeq database. Array scanning and generation of raw signal data files were done with GeneChip operating software (Affymetrix). Subsequent data analysis was done by GeneSpring (Agilent Technologies, CA) and DAVID bioinformatic resources 6.7 (NIH).

RESULTS

KDM4B·2·H3K9me3 Crystal Structure. In an effort to understand the detailed structure−function relationship of KDM4B at an atomic resolution, the recombinant catalytic domain of KDM4B was subjected to crystallization in the presence of a peptide, Ni(II), and AKG or compound **2**. After extensive trials, a well-diffracting crystal was found to consist of a large piece of residual density in the binding pocket, which could be modeled as the H3K9me3 peptide, compound **2**, and Ni (Figure 1A). The final crystal structure shows a 1.87 Å resolution monomer (R = 21.8%; R_{free} = 26.2%) that consists of the KDM4B catalytic domain (residues 9−337), compound **2**, and an H3K9me3 peptide (residues 7−14) within the active site (Table S2 of the Supporting Information). A Ni(II) ion is located on a site corresponding to the Fe(II) position on the bottom of the catalytic pocket. The JmjC domain of KDM4B folds into a β-jellyroll structure, characteristic of members in the KDM4 family (Figure 1B).[25] Superposition of KDM4A·**1**·H3K9me3 (PDB code: 2OQ6), KDM4B·**2**·H3K9me3, KDM4C·**1** (PDB code: 2XML), and KDM4D·AKG·H3K9me3 (PDB code: 4HON) shows limited conformational change in overall Cα atoms. The RMSD between KDM4A and KDM4B is 0.54 Å (residues 9−337 of KDM4B).

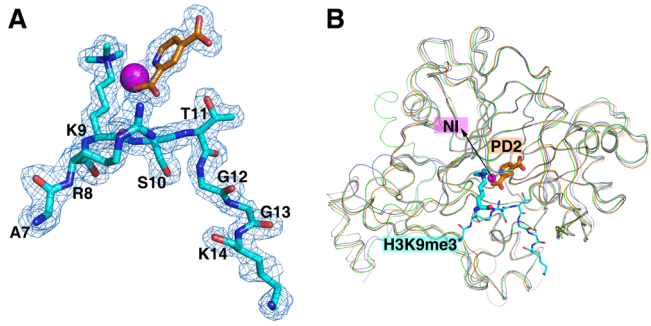

Figure 1. KDM4B·2·H3K9me3 crystal structure. (A) Electron density map for Ni(II), **2**, and H3K9me3 peptide. The $2F_o - F_c$ electron density maps are contoured at 1.0σ. (B) KDM4A (PDB code: 2OQ6), KDM4B (this study; PDB code: 4LXL), KDM4C (PDB code: 2XML), and KDM4D (PDB code: 4HON) are colored green, orange, blue, and gray, respectively. The stick models of compound **2** (pyridine 2,4-dicarboxylic acid) and the peptide are colored orange and cyan, respectively. Oxygen, nitrogen, and nickel atoms are colored red, blue, and magenta, respectively.

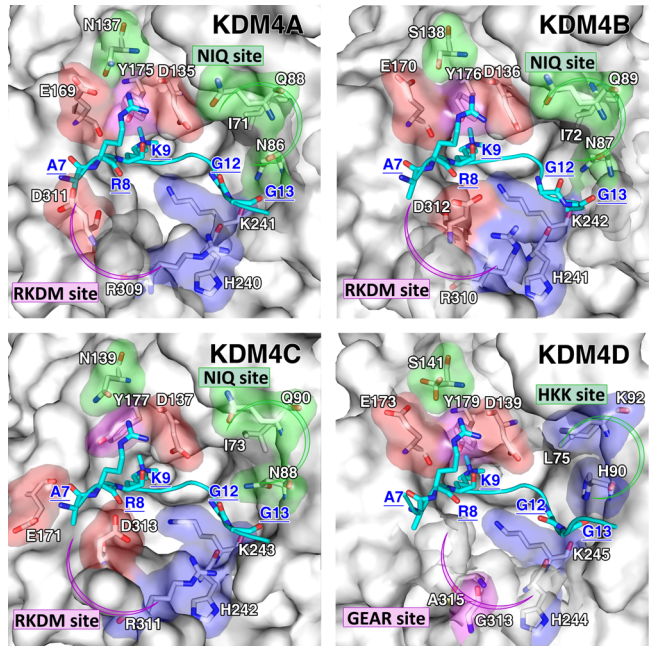

Figure 2. Differential ligand binding region between KDM4A/KDM4B/KDM4C and KDM4D. Superposition of KDM4A, KDM4B, KDM4C, and KDM4D reveals two heterogeneous regions, RKDM and NIQ. Surface representation of KDM4A, KDM4B, and KDM4D shows that the RKDM and NIQ regions and a crucial isoleucine (KDMA, I71; KDM4B, I72) make several contacts with the peptide at (−2) and (+3 and +4) sites in KDM4A and KDM4B. The corresponding GEAR and HKK sites deviate away from H3K9me3. The following PDB codes were used: 2OQ6 (KDM4A), 4LXL (KDM4B), and 4HON (KDM4D).

In the active site, compound **2** is situated at a position nearly overlapped with AKG in which one of its carboxyl moieties contacts H189, E191, and K242, while the other H bonds with Y133 and K207, similar to those that contact with AKG (Y132, N198, and K206 in KDM4A). Ni(II), which occupies the site of Fe(II), makes contacts with three strictly conserved residues

dx.doi.org/10.1021/jm500249n | J. Med. Chem. 2014, 57, 5975−5985

Table 1. Kinetic Parameters for KDM4A and KDM4B Using $H3_{3-17}$K9me3 or $H3_{31-41}$K36me3 as the Substrate

	$H3_{3-17}$K9me3		
KDM4	k_{cat} (s^{-1})	K_m (μM)	k_{cat}/K_m (s^{-1} μM^{-1})
KDM4A	0.017 ± 0.001	92.5 ± 5.9	1.8×10^{-4}
KDM4B	0.014 ± 0.001	88.3 ± 8.6	1.6×10^{-4}
	$H3_{31-41}$K36me3		
KDM4A	0.015 ± 0.001	169.9 ± 19.9	8.8×10^{-5}
KDM4B	0.013 ± 0.001	138.5 ± 14.1	9.4×10^{-5}

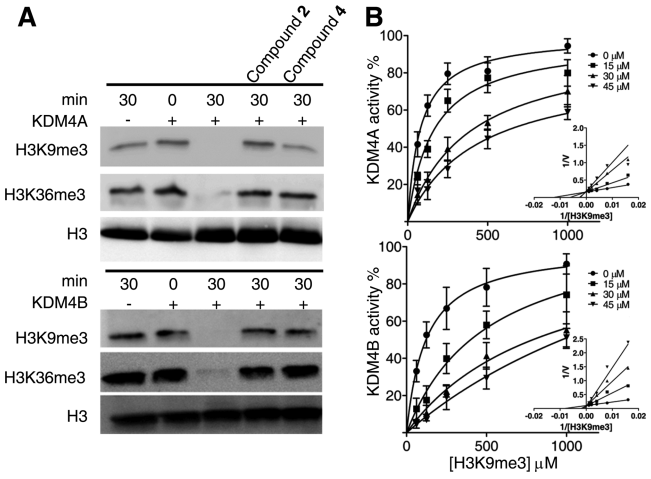

Figure 3. Compound **4** inhibits demethylase activity of KDM4A and KDM4B. (A) Demethylation of calf thymus H3 by bacteria-expressed KDM4A (upper panel) and KDM4B (lower panel) was determined in the presence of **4** by western blot analysis. The reaction mixture containing 10 μM enzyme, 100 μM inhibitor or blank buffer, and 5 μM of H3 in 50 mM HEPES, pH 7.5, 1 mM AKG, 2 mM ascorbate, and 50 μM Fe(II) was incubated at 37 °C for 30 min, followed by western blot analysis. H3 lysine modifications were probed with H3K9me3 and H3K36me3 antisera, respectively. (B) Inhibition kinetics of KDM4A/KDM4B demethylation activity by **4**. The inset in each panel shows the double-reciprocal form, where the 1/relative activity is plotted versus 1/[H3K9me3] at various fixed concentrations of the inhibitor.

(H189, E191, and H277 in KDM4B). G171, Y176, T290, and N291 in KDM4B, which surround the methylated lysine, are also strictly conserved (Figure S1 of the Supporting Information).

The most prominent feature of the KDM4 family is its potent catalytic activity toward H3K9me3/me2.[18,26] Analysis of superimposed H3K9me3 liganded structures including KDM4A, KDM4B, and KDM4D [KDM4A·Fe(II)·**1**·H3K9me3 (PDB code: 2OQ6), KDM4B·Ni(II)·**2**·H3K9me3 (this study; PDB code: 4LXL), KDM4D·Ni(II)·AKG·H3K9me3 (PDB code: 4HON)] reveals a conserved region to accommodate R8 (−1) and the methylated K9 of H3. Notably, three conserved residues (KDM4A: D135, E169, Y175; KDM4B: D136, E170, Y176; KDM4D: D139, E173, Y179) from β7 and β8 make H contacts with the guanidinium group of R8, the peptide O and N atoms of K9, and the peptide N atom of T11 from H3. In the interior of this cleft, a lysyl side chain (KDM4A: K241; KDM4B: K242; KDM4D: K245) forms a strong bond to the peptide O atom of S10 (Figure S1 of the Supporting Information), which together properly orient H3K9me3/me2 for similarly efficient catalysis in KDMs.[18] Interestingly, the KDM4A/KDM4B/KDM4C subfamily, but not KDM4D, exhibits additional specificity to demethylate H3K36me3/me2.[18,26] Consistent with the structural analysis for KDM4D,[18] we observe two heterogeneous regions in KDM4B that account for the substrate specificity: (1) RKDM versus GEAR and (2) NIQ versus HKK (Figure 2).

The RKDM site (residues 310−313 in KDM4B) from a long U-shaped loop resides near the (−1 and −2) site of the peptide-binding cleft. The aspartate side chain of RKDM (D311 in KDM4A) faces toward the peptide (−1 and −2 sites) and could make contacts with the peptide (Figure 2). Additionally, the long and positively charged side chain of R from RKDM contributes to contact with the plus side of the peptide, as demonstrated in two liganded structures: KDM4A·AKG·H3K9 (PDB code: 2Q8C) [KDM4A/R309 (NH1)−H3/G12 (O): 3.8 Å][27] and KDM4A·*N*-oxalylglycine·H3K36 (PDB code: 2P5B) [KDM4A/R309 (NH1)−H3/H39 (N): 3.8 Å].[25a] A subtle difference is also noted at the other side of this U loop between KDM4A and KDM4B; there is a T308−D236 contact in KDM4B but not in KDM4A (the corresponding residues are S307 and E235). In contrast, the GEAR motif deviates away from the peptide-binding cleft; hence, it makes no contacts with the peptide.

The other region is the NIQ site from the β4−β5 segment shared in KDM4A/KDM4B/KDM4C (residues 87−89 in KDM4B); KDM4D has HKK at the corresponding region. Q89 is noted to contact H3H39 and R40 (+3 and +4),[25a] whereas KDM4D consists of HKK with positively charged side chains at the corresponding site (Figure 2), which is likely to yield steric hindrance and electrostatic repulsion against H39 and R40 of H3K36me3.[18] I71, which is near NIQ (KDMA, I71; KDM4B, I72), also plays a crucial role.[18]

We used the FDH-demethylase coupled continuous fluorescent demethylase method[28] to assess the enzymatic activity of recombinant KDM4A and KDM4B expressed in *E. coli*. Using an H3K9me3 peptide (residues 3−17) as the substrate, KDM4A and KDM4B exhibited comparable catalytic activity (Table 1), consistent with Hillringhaus et al.[25b] We were able to measure the kinetic parameters with an H3K36me3 peptide ($H3_{31-41}$K36me3) and obtained an analogous k_{cat} value and a higher K_m value compared with those for the H3K9me3 peptide, suggesting that KDM4A/KDM4B have a lower binding affinity toward H3K36me3 than H3K9me3.

We further utilized calf thymus histones as the substrate and probed for H3K9, H3K27, and H3K36me3/me2/me1 in the presence of recombinant KDM4A or KDM4B using western blot analysis. As shown in Figure S2, the signal of H3K9me3/me2 was significantly reduced and that of H3K9me1 was increased in the presence KDM4A (upper panel) or KDM4B (lower panel) in a time-dependent manner compared with that in the controls, indicating that an active KDM4A/KDM4B forms to remove the methyl group from H3K9me3/me2. For the H3K36 signal, a longer time was needed to remove the signal for H3K36me3/me2. No difference was found for H3K27me3 or H3K27me1. These results collectively suggest that KDM4A and KDM4B demethylate H3K9me3/me2 more efficiently than H3K36me3/me2 and that there was no activity toward H3K27me3/me2/me1, confirming our results in Table 1.

Virtual Screening To Identify 4 as a Novel Active-Site Inhibitor toward KDM4A and KDM4B. We utilized GEMDOCK[22] to screen for putative hits against the NCI database. The known inhibitor **2** was used as a positive control,

dx.doi.org/10.1021/jm500249n | J. Med. Chem. 2014, 57, 5975−5985

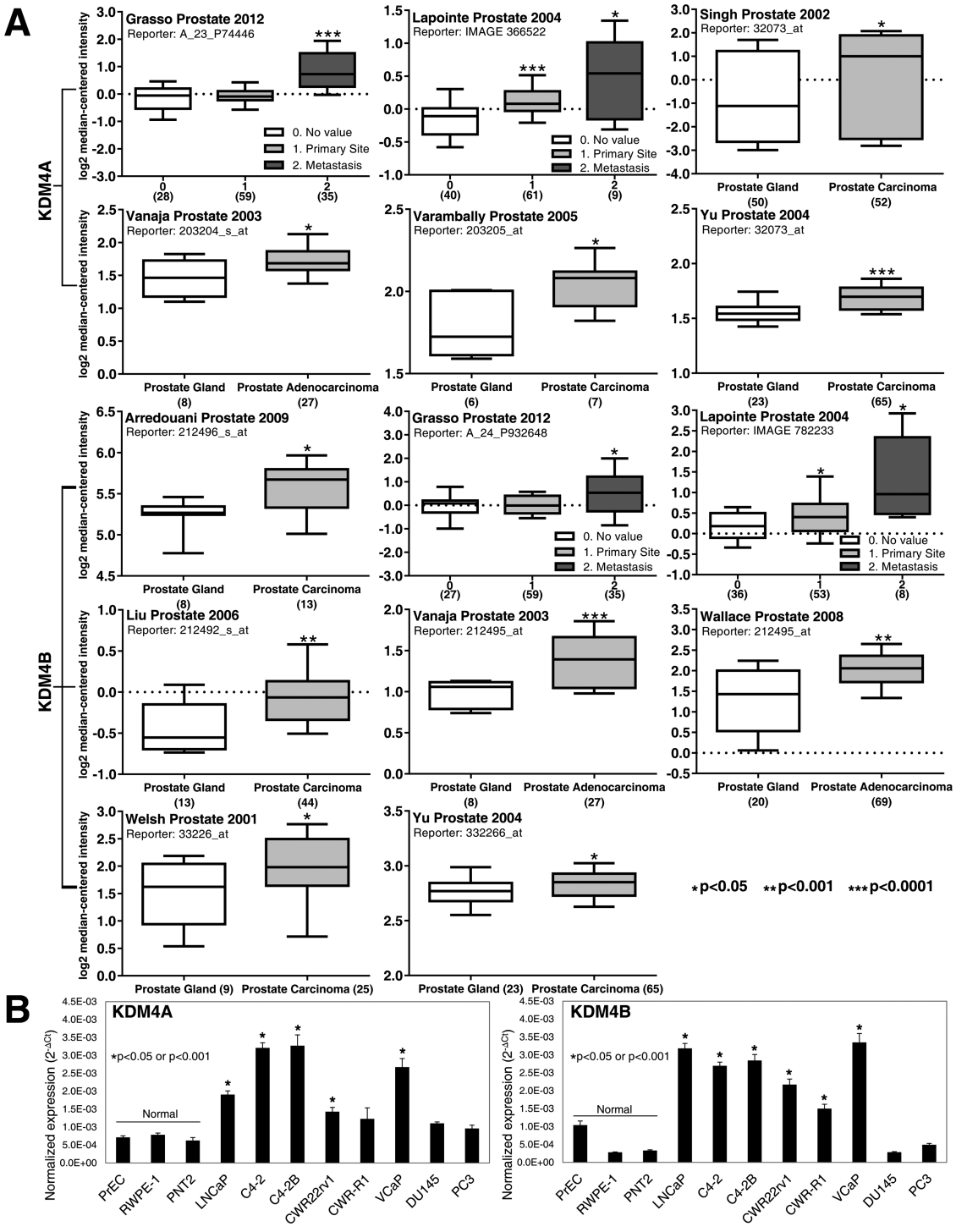

Figure 4. KDM4A and KDM4B are highly expressed in prostate cancer cells. (A) Expression values of KDM4A and KDM4B in normal prostate glands and tumor tissues from the selected studies were obtained from the Oncomine (Compendia Bioscience, Ann Arbor, MI, USA) database (http://www.oncomine.org/). The box and whisker plots show a box that encompasses the 25th−75th percentiles, the median as a line within the box, and the 10th and 90th percentiles as error bars. *p* values were determined by one-tailed Student's *t* test and were calculated on the basis of the comparison of normal vs cancer; normal vs primary sites; or normal vs metastasis. (B) qRT-PCR analysis of KDM4A and KDM4B expression in normal prostate primary cells (PrEC), normal prostate epithelial cell lines (RWPE-1 and PNT2), and prostate cancer cell lines (LNCaP, C4-2, C4-2B, CWR22rv1, CWR-R1, VCaP, DU145, and PC3). Asterisks indicate significant overexpression compared to that in normal cells.

which showed significant inhibition [21% (KDM4A) and 24% (KDM4B) of residual activity].[29] We selected 10 compounds from the top-ranked 3000 compounds based on their ranking, availability, domain knowledge, and docked-pose analysis (Table S1). Of these, compound **4**, which was docked into the active site (Figure S3), exhibited the highest inhibitory effect toward both KDM4A (28%) and KDM4B (35%) (Table S1). To confirm the FDH-demethylase coupled results, we utilized histones as the substrate and probed for H3K9me3 and H3K36me3 in the absence or presence of recombinant

dx.doi.org/10.1021/jm500249n | J. Med. Chem. 2014, 57, 5975−5985

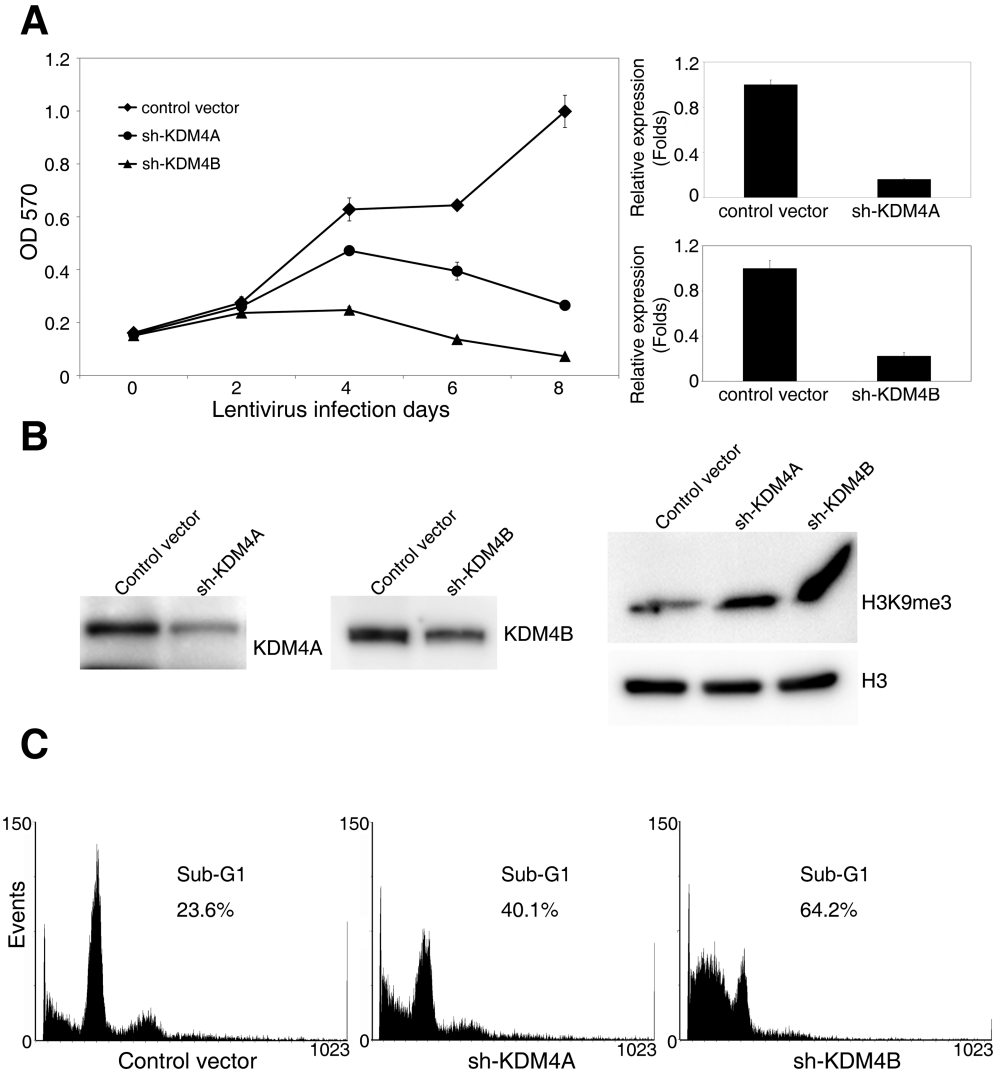

Figure 5. (A) KDM4A and KDM4B are crucial for the growth of LNCaP cells. LNCaP cells were infected with lentivirus encoding control shRNA (control), sh-KDM4A, or sh-KDM4B, as indicated (left panel). qRT-PCR analysis was performed to evaluate the expression of KDM4s (right panel). (B) H3K9me3 levels in KDM4A and KDM4B knockdown cells. LNCaP cells were infected by lentivius carrying control vector, sh-KDM4A, or sh-KDM4B for 3 days. The KDM4A, KDM4B, and H3K9me3 signals were detected in cell lysates by western blot analysis as indicated. (C) Flow cytometry analysis of the DNA content in sh-KDM4A and sh-KDM4B LNCaP cells.

KDM4A or KDM4B using western blot analysis. Figure 3A shows that compounds **2** and **4** indeed blocked the demethylation activity. Further kinetic inhibition characterization of compound **4** demonstrated a competitive inhibitory mode against $H3_{3-17}K9me3$ for KDM4A [IC_{50} = 6.4 μM; K_i (H3K9me3) = 5.5 ± 1.6 μM; Figure 3B). KDM4B also showed analogous inhibition kinetics [IC_{50} = 9.3 μM; K_i (H3K9me3) = 3.0 ± 1.1 μM).

We next tested whether compound **4** could inhibit purified, recombinant KDM4D and KDM4E. Using the in vitro FDH-demethylase coupled assay, compound **4** exhibited a much weaker inhibitory effect toward KDM4D and KDM4E than did compound **2** (Figure S4A). We further characterized the methylated status of H3 in LNCaP cells treated with compound **4**. As shown in Figure S4B, only the level of H3K9me3 was significantly increased in compound **4**-treated LNCaP cells as opposed to essentially comparable signals of H3K4me2, H3K27me3, H3K27me2, H3K36me3, H3K36me2, and H3K79me2 between control and treated cells. Together, these provide strong evidence that compound **4** is a potent, selective inhibitor against H3K9me3 demethylation by KDM4A/KDM4B in LNCaP cells.

Genetic and Pharmacological Inhibition of KDM4A and KDM4B Induces Apoptosis. Several studies have reported that KDM4 family members are overexpressed in various cancers.[3b] To further support the clinical relevance of KDM4A and KDM4B in prostate cancer, we took advantage of the comprehensive database collection of OncomineTM (Compendia Bioscience, Ann Arbor, MI, USA) (http://www.oncomine.org/) to examine their expression profiles between normal prostate glands and tumor tissues. Among the 14 data sets available, a statistically significant (p < 0.05) elevation of KDM4A was seen in 6 data sets and KDM4B was elevated in 8 data sets in prostate cancer (PCa) compared to their levels in normal/benign samples (Figure 4A). The rest of the data sets also exhibited higher median values of KDM4A/KDM4B expression in PCa sites, despite not being statistically significant (Figure S5). Strikingly, the level of KDM4A and KDM4B expression is positively correlated with prostate cancer progression (normal, primary PCa, and metastatic PCa).[30]

dx.doi.org/10.1021/jm500249n | J. Med. Chem. 2014, 57, 5975−5985

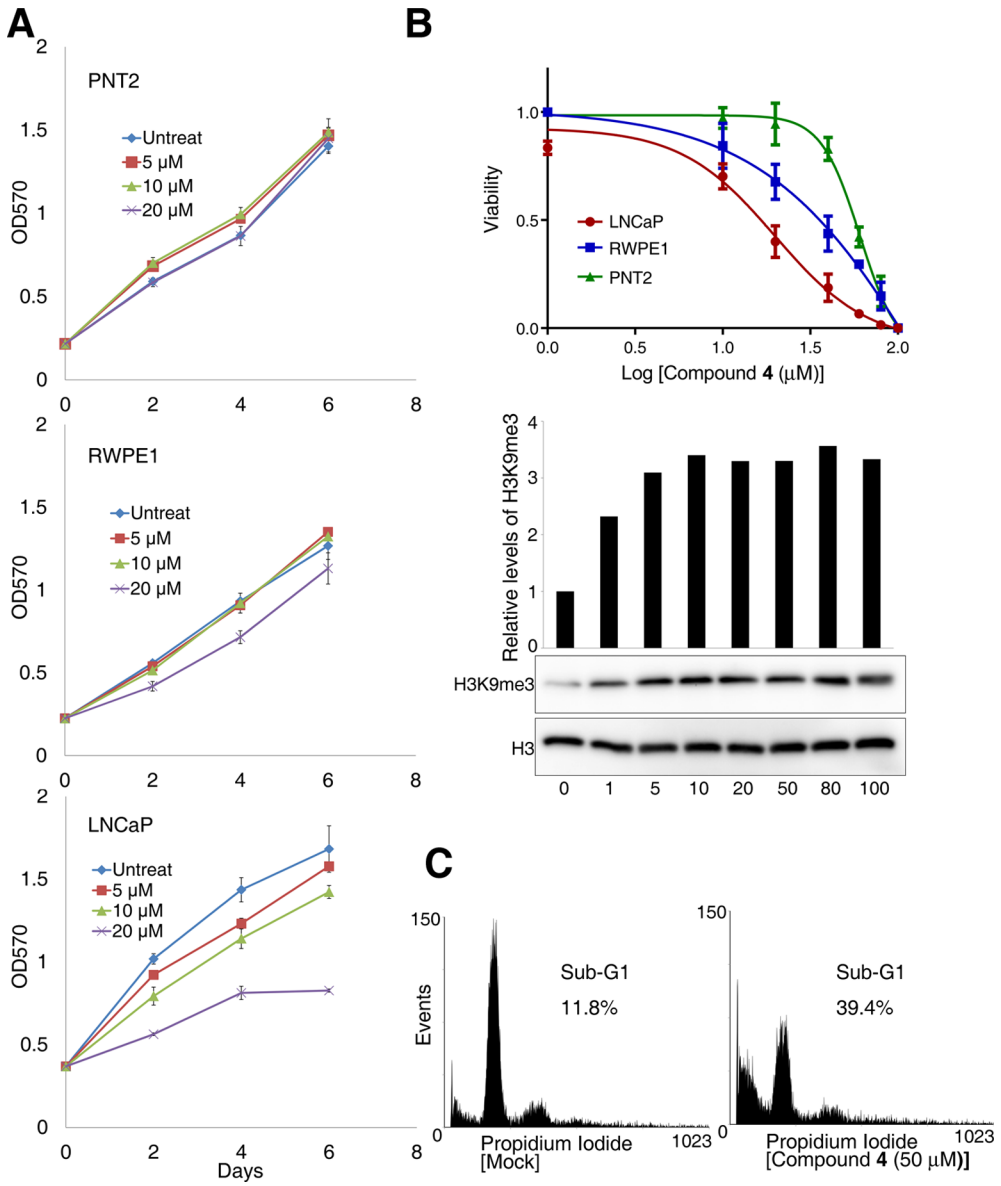

Figure 6. Compound **4** exhibits anticancer effects on LNCaP cells. (A) Treatment of LNCaP or normal prostate (PNT2 and RWPE1) cells with different concentrations of inhibitor **4** over 5 days shows inhibitor **4**'s selective anticancer properties toward LNCaP cells. (B) Inhibition of viability by inhibitor **4** in normal prostate and LNCaP cells. LNCaP and normal prostate (PNT2 and RWPE1) cells were treated with inhibitor **4** for 3 days, and viability was measured by viable cell count. Standard deviation is derived from biological triplicates. The H3K9me3 signal (lower panel) was detected in cell lysates treated with different concentrations (1−100 μM) of inhibitor **4** for 24 h, followed by estern blot analysis using anti-H3K9me3 antibody. The different concentrations (1−100 μM) of inhibitor **4** are indicated below the blot. The level of H3K9me3 was detected and quantified by AlphaView SA (Cell Biosciences Inc.). The level of H3K9me3 is shown by bar graph. (C) Flow cytometry analysis of the DNA content in LNCaP cells treated with DMSO (mock) or 50 μM inhibitor **4** for 3 days.

We also examined the expression of KDM4A and KDM4B in several laboratory-cultured prostate cancer cell models: normal prostate epithelial cells (PrEC, RWPE-1, and PNT2) and a number of prostate cancer cell lines (LNCaP, C4-2, C4-2B, CWR22rv1, CWR-R1, VCaP, DU145, and PC3). Essentially, all prostate cancer cells exhibited higher expression of KDM4A compared with its level in normal prostate epithelial cell lines, which was statistically significant for LNCaP, C4-2, C4-2B, CWR22rv1, and VCaP cells (Figure 4B). Similarly, with the exceptions of DU145 and PC3, KDM4B is overexpressed in all other malignant cell lines tested.

To assess whether KDM4A or KDM4B was crucial for prostate cancer cell growth, LNCaP cells were treated with sh-KDM4A or sh-KDM4B to knockdown the expression of KDM4A or KDM4B, respectively (Figure 5A). A significantly reduced level of cell growth was found in KDM4A and KDM4B knockdown cells (Figure 5A). Correspondingly, there was an increased level of H3K9me3 signal in either of KDM4A or KDM4B knockdown cells (Figure 5B). Flow cytometry analysis showed that there was a significantly increased population of apoptotic cells in sh-KDM4A (40.1%) or sh-KDM4B (64.2%) cells compared to that in control cells (23.6%) (Figure 5C). These results suggest that KDM4A and KDM4B are critical to the viability of the cancer cells and thus are potentially useful targets for intervention.

The knockdown data for KDM4A and KDM4B prompted us to test whether compound **4**, which inhibits both KDM4A and KDM4B, would similarly reduce the viability of LNCaP cells.

dx.doi.org/10.1021/jm500249n | J. Med. Chem. 2014, 57, 5975−5985

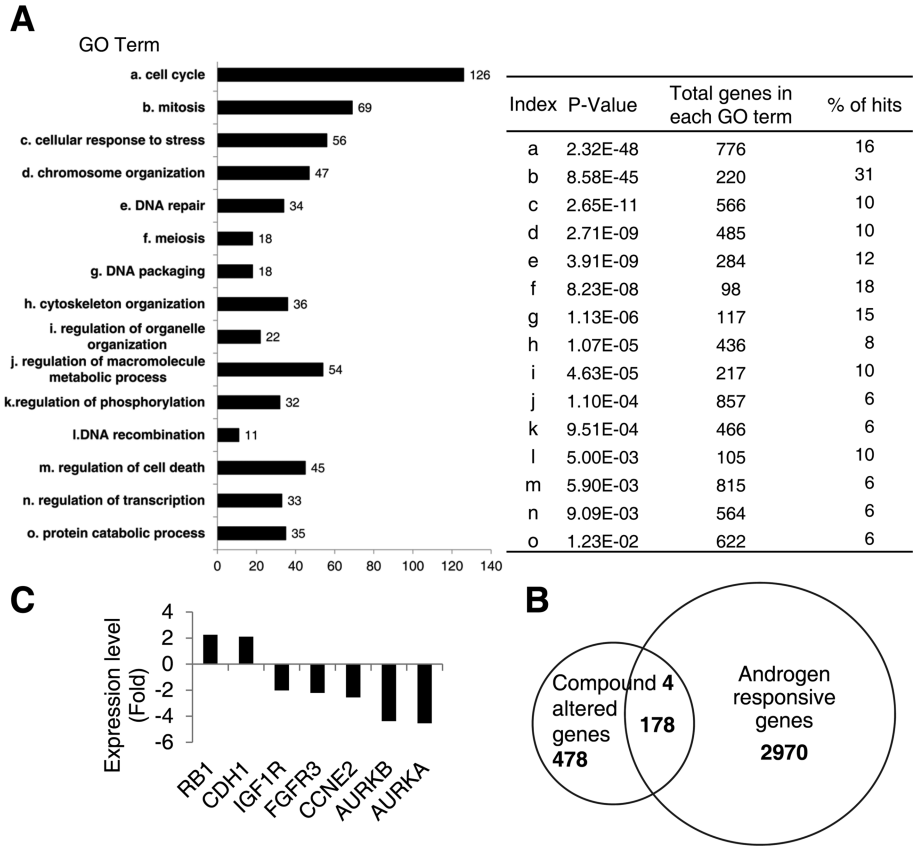

Figure 7. Microarray analysis of LNCaP cells treated with inhibitor **4** (50 μM) compared to that of mock-treated cells. (A) DAVID functional annotation of the genes that showed 2-fold alterations in expression. GO terms associated with the altered genes that show statistically strong enrichment with low p values are listed. The numbers next to each bar in the graph indicate the gene count for each pathway. Percent of hits indicates the percentage of genes that are altered in each GO classification. (B) Expression of tumor suppressors and oncogenes that are up- and downregulated in the inhibitor-treated cells, respectively. (C) Venn diagram of the overlap of the inhibitor-altered genes with androgen-responsive genes.

Figure 6A shows that this compound had hardly any effect on PNT2 cells over 6 days (5–20 μM), whereas there was slightly reduced growth for the other normal cell line, RWPE1, upon 20 μM treatment. By contrast, the growth of LNCaP cells was significantly affected by inhibitor **4**. As shown in Figure 6B, inhibitor **4** effectively kills LNCaP cells after 3 day culture (cytotoxicity IC_{50} = 16.5 μM). To validate the effect of inhibitor **4**, we examined the cellular level of H3K9me3 in the treated cells. Inhibitor **4**-treated cells had a notable increase in the level of H3K9me3 in a dose-dependent manner: 5 μM inhibitor **4** treatment almost completely blocked the demethylating activity toward H3K9me3. Flow cytometry analysis showed that there were nearly 4-fold more apoptotic LNCaP cells produced upon treatment with inhibitor **4** compared to that for mock-treated cells (11.9 vs 39.5%) (Figure 6C). These results collectively suggest that inhibition of KDM4A/KDM4B by shRNA or by inhibitor **4** specifically inhibits the demethylating activity of H3K9me3 and strongly blocks cell growth. As a comparison, we utilized the dimethyl ester form of compound **2**, the most potent inhibitor against KDM4E (in vitro assay), which allows penetration into the cells.[10] Consistent with the other results, a high CC_{50} value was found in LNCaP cells treated with **2** (588.7 μM).

Inhibition of KDM4 by 4 Negatively Regulates AR Responsive Genes. To understand the mechanisms associated with growth inhibition and apoptosis induction by inhibitor **4**, we characterized the differential gene expression profiles in LNCaP cells treated with or without **4** using microarray analysis (≥2-fold alterations). As shown in Figure 7A, functional annotations indicated a number of differentially expressed genes related to cell division and DNA processes. Most intriguingly, a significant portion (27% = 178/656) of the altered genes were found to be androgen-responsive genes (Figure 7B). In addition to the alteration of androgen-responsive genes, inhibitor **4** induced upregulation of tumor suppressors RB1 and CDH1 as well as downregulation of oncogenes IGF1R, FGFR3, CCNE2, AURKA, and AURKB (Figure 7C), which may contribute to a loss of proliferation and survival advantages for the tumor cell. The mRNA expression of AR-signature genes was shown in Figure 8.

We further compared the expression profiles of selected AR-responsive genes (CDC6, CDC25A, CLDN8, FZD3, KLK3, MCM5, NKX3.1, RRM2, TMEPA1, and TMPRSS2) in two sets of experiments using qRT-PCR analysis: (i) control, sh-KDM4A, and sh-KDM4B cells and (ii) control and **4**-treated LNCaP cells (Figure S6). Overall, there were similarly downregulated expression profiles for these genes in cells treated with inhibitor **4**, sh-KDM4A, and sh-KDM4B, indicating that the targets of inhibitor **4** were indeed KDM4A/KDM4B. This is also consistent with previous results showing that both KDM4A and KDM4B (as well as KDM4C) are coactivators of AR.[5] Thus, inhibitor **4** specifically inhibits the expression of genes involved in DNA-dependent processes, cell proliferation, and AR-dependent signaling in prostate

dx.doi.org/10.1021/jm500249n | J. Med. Chem. 2014, 57, 5975–5985

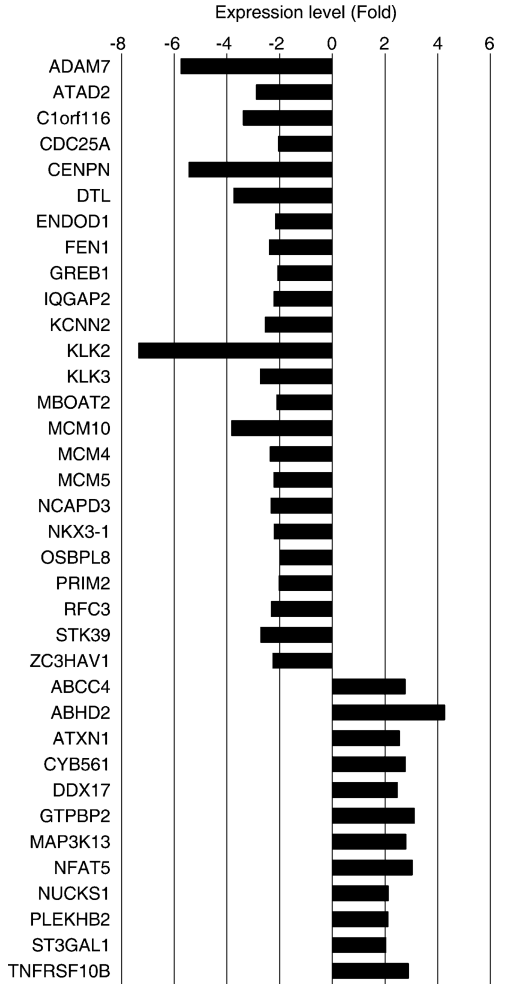

Figure 8. AR-signature genes are differentially expressed in inhibitor **4**-treated LNCaP cells.

cancer cells. Given the importance of AR in prostate carcinogenesis, compounds that inhibit KDM4A and KDM4B may be beneficially used to overcome castration-resistant prostate cancer.

DISCUSSION

In this study, we report a peptide-liganded KDM4B structure that demonstrates a well-conserved core active site with that of KDM4A and KDM4C, supporting the efficient catalytic power of this subfamily to demethylate both H3K9me3/me2 and H3K36me3/me2. This structure also presents two heterogeneous regions in the peptide-binding cleft compared with that of KDM4D, which accounts for the sole H3K9me3, but not H3K36me3, specificity of KDM4D: (i) RKDM vs GEAR and (ii) NIQ vs HKK.

Importantly, we identified an inhibitor, **4**, that selectively blocks in vitro demethylation activity (H3K9me3 and H3K36me3) by KDM4A/KDM4B based on a virtual structure-guided screening method.[22a,31] Compound **4** also significantly inhibits histone demethylase activity on H3K9me3 and induces apoptosis in cultured LNCaP cells. Knocking down KDM4B expression by shRNA treatment also reduces the viability of LNCaP cells. This inhibitory effect appears to be largely due to its transcriptional reprogramming of genes that control cell proliferation, particularly those involved in the cell cycle and mitosis. Also affected are genes involved in DNA repair, DNA recombination, and chromosomal organization, suggesting that KDM4 plays a role in regulating genome stability. Our results are echoed by a recent report that KDM4A overexpression leads to genomic amplification.[32] Perhaps the most striking finding of the microarray analysis is that a significant portion (close to ∼30%) of **4**-altered genes are androgen-responsive, consistent with the roles of KDM4A−C as critical coactivators of AR and suggesting its potential to be used to treat castration-resistant prostate cancer. Furthermore, compound **4** exhibits a competitive inhibitory mode against the H3K9me3 peptide. It specifically blocked KDM4A/KDM4B but only weakly suppressed KDM4D and KDM4E. Importantly, cell-based results revealed that compound **4**-treated LNCaP cells significantly lost demethylation capability toward H3K9me3 but not toward other methyl marks (H3K4me2, H3K27me3, H3K27me2, H3K36me3, H3K36me2, and H3K79me2). Together, these provide strong evidence that compound **4** is a potent, selective inhibitor against H3K9me3 demethylation by KDM4A/KDM4B in LNCaP cells.

Much attention has been focused on developing KDM4-targeted inhibitors because of their importance in biological processes including carcinogenesis.[33] Currently, the developed inhibitors include analogues of **1**−**3** that all occupy the AKG site (PDB codes: 2P58, 2VD7, and 3NJY). Despite the high potencies demonstrated by these inhibitors in vitro, their clinical outcomes are not yet clear. A recent cell-based screening study reported a potent pan-selective inhibitor, JIB-04, a nonsymmetrical pyridine hydrazone that consists of E and Z isomers. It is noted that its E isomer (not Z) shows pan inhibition toward JmjC-containing KDMs in vitro and anticancer effects in cells and in a breast cancer model.[34] However, this molecule also blocks prolyl hydroxylase, albeit weakly, and thus may have more global effects on cells than intended. Inhibitor **4**, although not as potent as JIB-04, offers a new structural framework that lies on the selective peptide-binding region apart from the AKG site. Further structure−activity relationship (SAR) studies on JIB-04 and **4** are thus likely to contribute to the development of new selective agents against KDM-dependent functions.

In summary, inhibition of KDM4A/KDM4B by pharmacological (inhibitor **4**) or genetic (sh-KDM4A and sh-KDM4B) means selectively downmodulates cell growth-promoting genes, including androgen-responsive genes, resulting in the effective killing of prostate cancer cells. To our knowledge, this is the first KDM4A/KDM4B inhibitor that shows anticancer properties in prostate cancer cells. This inhibitor thus provides an attractive scaffold for further SAR development of new KDM4 modulators to control its coactivation for transcriptional programming of prostate cancer cells.

ASSOCIATED CONTENT

Supporting Information

Binding pocket analysis in KDM4s (Figure S1); western blot of KDM4A and KDM4B that demethylate H3K9me3/me2 and H3K36me3/me2 but not H3K27me3 (Figure S2); superposition of the KDM4B·**2**·H3K9me3 structure and the KDM4B·**4** docked pose (Figure S3); selective inhibitory effect of compound **4** (Figure S4); KDM4A and KDM4B expression data in PCa sites (Figure S5); downregulation of AR target genes in KDM4A/KDM4B-knockdown and compound **4**-treated cells (Figure S6); inhibition effects of selected hits on KDM4A and KDM4B (Table S1); and crystallographic data and refinement statistics for KDM4B·**2**·H3K9me3 (Table S2).

dx.doi.org/10.1021/jm500249n | J. Med. Chem. 2014, 57, 5975−5985

This material is available free of charge via the Internet at http://pubs.acs.org.

Accession Codes

The atomic coordinates of KDM4B have been deposited as Protein Data Bank entry 4LXL.

AUTHOR INFORMATION

Corresponding Authors

*(J.-M.Y.) E-mail: moon@faculty.nctu.edu.tw; Phone: +886-3-5715131 (ext 56942); Fax: +886-3-5729288.

*(H.-J.K.) E-mail: hkung@nhri.org.tw; Phone: +886-3-7246166 (ext 31000); Fax: +886-3-7586402.

*(W.-C.W.) E-mail: wcwang@life.nthu.edu.tw and wenching.wc@gmail.com; Phone: +886-3-5742766; Fax: +886-3-5742766 and +886-3-5717237.

Author Contributions

#C.-H.C., L.-Y.W., and K.-C.H. are co-first authors.

Notes

The authors declare no competing financial interest.

ACKNOWLEDGMENTS

This work was supported by NSC, Taiwan (NSC102-2321-B-007−003 and NSC102-2325-B-007−001), and by "Aim for the Top University Project" of NTHU and MOE, Taiwan, ROC. We acknowledge the support of grants from the NIH, USA, as well as NHRI (02A1MGPP20-014) and MOHW (DOH102-TD-M-111-100001), Taiwan, to H.-J.K. We thank the Macromolecular X-ray Crystallographic Center at the National Tsing Hua University Instrument Center at Hsinchu, Taiwan, for access to the BL13B1 beamline at NSRRC, Taiwan, and the SP12B2 Taiwan beamline at SPring-8, Japan, for data collection. We also thank the staff at NSRRC for their excellent support.

ABBREVIATIONS USED

AKG, α-ketoglutarate; JmjC, Jumonji C; AR, androgen receptor of KDM4s; ER, estrogen receptor of KDM4A and B; OGA, *N*-oxalylglycine; PD2, 2,4-dicarboxylic acids; 8HQ, 8-hydroxyquinolines; DE3, *Escherichia coli* BL21; IPTG, isopropyl-β-D-thiogalactopyranoside; DMSO, dimethyl sulfoxide; ascorbate, ascorbic acid; PEG, poly(ethylene glycol); RMSD, root-mean-squared deviation; FDH, formaldehyde dehydrogenase; PCa, prostate cancer

REFERENCES

(1) (a) Shi, Y.; Lan, F.; Matson, C.; Mulligan, P.; Whetstine, J. R.; Cole, P. A.; Casero, R. A. Histone demethylation mediated by the nuclear amine oxidase homolog LSD1. *Cell* **2004**, *119*, 941−53. (b) Kouzarides, T. Chromatin modifications and their function. *Cell* **2007**, *128*, 693−705. (c) Mosammaparast, N.; Shi, Y. Reversal of histone methylation: biochemical and molecular mechanisms of histone demethylases. *Annu. Rev. Biochem.* **2010**, *79*, 155−79.

(2) (a) Breccia, M.; Alimena, G. NFκB as a potential therapeutic target in myelodysplastic syndromes and acute myeloid leukemia. *Expert Opin. Ther. Targets* **2010**, *14*, 1157−76. (b) Rodriguez-Paredes, M.; Esteller, M. Cancer epigenetics reaches mainstream oncology. *Nat. Med.* **2011**, *17*, 330−9. (c) Chi, P.; Allis, C. D.; Wang, G. G. Covalent histone modifications–miswritten, misinterpreted and mis-erased in human cancers. *Nat. Rev. Cancer* **2010**, *10*, 457−69.

(3) (a) Kampranis, S. C.; Tsichlis, P. N. Histone demethylases and cancer. *Adv. Cancer Res.* **2009**, *102*, 103−69. (b) Wang, L.-Y.; Guo, W.; Kim, K.; Pochampalli, M.; Hung, C.-L.; Izumiya, Y.; Kung, H.-J. Histone demethylases in prostate cancer. In *Nuclear Signaling Pathways and Targeting Transcription in Cancer*; Kumer, R., Ed; Springer Science +Business Media: New York, 2013.

(4) (a) Katoh, M.; Katoh, M. Identification and characterization of JMJD2 family genes in silico. *Int. J. Oncol.* **2004**, *24*, 1623−8. (b) Berry, W. L.; Janknecht, R. KDM4/JMJD2 histone demethylases: epigenetic regulators in cancer cells. *Cancer Res.* **2013**, *73*, 2936−42.

(5) (a) Shin, S.; Janknecht, R. Activation of androgen receptor by histone demethylases JMJD2A and JMJD2D. *Biochem. Biophys. Res. Commun.* **2007**, *359*, 742−6. (b) Wissmann, M.; Yin, N.; Muller, J. M.; Greschik, H.; Fodor, B. D.; Jenuwein, T.; Vogler, C.; Schneider, R.; Gunther, T.; Buettner, R.; Metzger, E.; Schule, R. Cooperative demethylation by JMJD2C and LSD1 promotes androgen receptor-dependent gene expression. *Nat. Cell Biol.* **2007**, *9*, 347−53. (c) Coffey, K.; Rogerson, L.; Ryan-Munden, C.; Alkharaif, D.; Stockley, J.; Heer, R.; Sahadevan, K.; O'Neill, D.; Jones, D.; Darby, S.; Staller, P.; Mantilla, A.; Gaughan, L.; Robson, C. N. The lysine demethylase, KDM4B, is a key molecule in androgen receptor signalling and turnover. *Nucleic Acids Res.* **2013**, *41*, 4433−46.

(6) (a) Shi, L.; Sun, L.; Li, Q.; Liang, J.; Yu, W.; Yi, X.; Yang, X.; Li, Y.; Han, X.; Zhang, Y.; Xuan, C.; Yao, Z.; Shang, Y. Histone demethylase JMJD2B coordinates H3K4/H3K9 methylation and promotes hormonally responsive breast carcinogenesis. *Proc. Natl. Acad. Sci. U.S.A.* **2011**, *108*, 7541−6. (b) Kawazu, M.; Saso, K.; Tong, K. I.; McQuire, T.; Goto, K.; Son, D. O.; Wakeham, A.; Miyagishi, M.; Mak, T. W.; Okada, H. Histone demethylase JMJD2B functions as a co-factor of estrogen receptor in breast cancer proliferation and mammary gland development. *PLoS One* **2011**, *6*, e17830. (c) Berry, W. L.; Shin, S.; Lightfoot, S. A.; Janknecht, R. Oncogenic features of the JMJD2A histone demethylase in breast cancer. *Int. J. Oncol.* **2012**, *41*, 1701−6.

(7) (a) Hamada, S.; Kim, T. D.; Suzuki, T.; Itoh, Y.; Tsumoto, H.; Nakagawa, H.; Janknecht, R.; Miyata, N. Synthesis and activity of N-oxalylglycine and its derivatives as Jumonji C-domain-containing histone lysine demethylase inhibitors. *Bioorg. Med. Chem. Lett.* **2009**, *19*, 2852−5. (b) Rose, N. R.; Woon, E. C.; Kingham, G. L.; King, O. N.; Mecinovic, J.; Clifton, I. J.; Ng, S. S.; Talib-Hardy, J.; Oppermann, U.; McDonough, M. A.; Schofield, C. J. Selective inhibitors of the JMJD2 histone demethylases: combined nondenaturing mass spectrometric screening and crystallographic approaches. *J. Med. Chem.* **2010**, *53*, 1810−8.

(8) Thalhammer, A.; Mecinovic, J.; Loenarz, C.; Tumber, A.; Rose, N. R.; Heightman, T. D.; Schofield, C. J. Inhibition of the histone demethylase JMJD2E by 3-substituted pyridine 2,4-dicarboxylates. *Org. Biomol Chem.* **2011**, *9*, 127−35.

(9) King, O. N.; Li, X. S.; Sakurai, M.; Kawamura, A.; Rose, N. R.; Ng, S. S.; Quinn, A. M.; Rai, G.; Mott, B. T.; Beswick, P.; Klose, R. J.; Oppermann, U.; Jadhav, A.; Heightman, T. D.; Maloney, D. J.; Schofield, C. J.; Simeonov, A. Quantitative high-throughput screening identifies 8-hydroxyquinolines as cell-active histone demethylase inhibitors. *PLoS One* **2010**, *5*, e15535.

(10) Mackeen, M. M.; Kramer, H. B.; Chang, K. H.; Coleman, M. L.; Hopkinson, R. J.; Schofield, C. J.; Kessler, B. M. Small-molecule-based inhibition of histone demethylation in cells assessed by quantitative mass spectrometry. *J. Proteome Res.* **2010**, *9*, 4082−92.

(11) Bradford, M. M. A rapid and sensitive method for the quantitation of microgram quantities of protein utilizing the principle of protein-dye binding. *Anal. Biochem.* **1976**, *72*, 248−54.

(12) Otwinowski, Z.; Minor, W. Processing of X-ray diffraction data collected in oscillation mode. *Methods Enzymol.* **1997**, *276*, 307−26.

(13) (a) Collaborative Computational Project. The CCP4 suite: programs for protein crystallography. *Acta Crystallogr., Sect. D: Biol. Crystallogr.* **1994**, *50*, 760−3. (b) Murshudov, G. N.; Vagin, A. A.; Dodson, E. J. Refinement of macromolecular structures by the maximum-likelihood method. *Acta Crystallogr., Sect. D: Biol. Crystallogr.* **1997**, *53*, 240−55.

(14) Vagin, A.; Teplyakov, A. MOLREP: an automated program for molecular replacement. *J. Appl. Crystallogr.* **1997**, *30*, 1022−5.

(15) Lamzin, V.; Wilson, K. S. Automated refinement of protein models. *Acta Crystallogr., Sect. D: Biol. Crystallogr.* **1993**, *49*, 127−47.

(16) Laskowski, R. A.; MacArthur, M. W.; Moss, D. S.; Thornton, J. M. PROCHECK: a program to check the stereochemical quality of protein structures. *J. Appl. Crystallogr.* **1993**, *26*, 283−91.
(17) Chen, Z.; Zang, J.; Kappler, J.; Hong, X.; Crawford, F.; Wang, Q.; Lan, F.; Jiang, C.; Whetstine, J.; Dai, S.; Hansen, K.; Shi, Y.; Zhang, G. Structural basis of the recognition of a methylated histone tail by JMJD2A. *Proc. Natl. Acad. Sci. U.S.A.* **2007**, *104*, 10818−23.
(18) Krishnan, S.; Trievel, R. C. Structural and functional analysis of JMJD2D reveals molecular basis for site-specific demethylation among JMJD2 demethylases. *Structure* **2013**, *21*, 98−108.
(19) Jones, T. A.; Zou, J. Y.; Cowan, S. W.; Kjeldgaard, M. Improved methods for building protein models in electron density maps and the location of errors in these models. *Acta Crystallogr., Sect. A* **1991**, *47*, 110−9.
(20) Raghuraman, A.; Mosier, P. D.; Desai, U. R. Finding a needle in a haystack: development of a combinatorial virtual screening approach for identifying high specificity heparin/heparan sulfate sequence(s). *J. Med. Chem.* **2006**, *49*, 3553−62.
(21) Chowdhury, R.; Yeoh, K. K.; Tian, Y. M.; Hillringhaus, L.; Bagg, E. A.; Rose, N. R.; Leung, I. K.; Li, X. S.; Woon, E. C.; Yang, M.; McDonough, M. A.; King, O. N.; Clifton, I. J.; Klose, R. J.; Claridge, T. D.; Ratcliffe, P. J.; Schofield, C. J.; Kawamura, A. The oncometabolite 2-hydroxyglutarate inhibits histone lysine demethylases. *EMBO Rep.* **2011**, *12*, 463−9.
(22) (a) Hsu, K. C.; Chen, Y. F.; Lin, S. R.; Yang, J. M. iGEMDOCK: a graphical environment of enhancing GEMDOCK using pharmacological interactions and post-screening analysis. *BMC Bioinformatics* **2011**, *12*, S33. (b) Yang, J. M.; Chen, C. C. GEMDOCK: a generic evolutionary method for molecular docking. *Proteins: Struct., Funct., Bioinf.* **2004**, *55*, 288−304.
(23) Gregory, C. W.; Johnson, R. T., Jr.; Mohler, J. L.; French, F. S.; Wilson, E. M. Androgen receptor stabilization in recurrent prostate cancer is associated with hypersensitivity to low androgen. *Cancer Res.* **2001**, *61*, 2892−8.
(24) Thalmann, G. N.; Anezinis, P. E.; Chang, S. M.; Zhau, H. E.; Kim, E. E.; Hopwood, V. L.; Pathak, S.; von Eschenbach, A. C.; Chung, L. W. Androgen-independent cancer progression and bone metastasis in the LNCaP model of human prostate cancer. *Cancer Res.* **1994**, *54*, 2577−81.
(25) (a) Chen, Z.; Zang, J.; Whetstine, J.; Hong, X.; Davrazou, F.; Kutateladze, T. G.; Simpson, M.; Mao, Q.; Pan, C. H.; Dai, S.; Hagman, J.; Hansen, K.; Shi, Y.; Zhang, G. Structural insights into histone demethylation by JMJD2 family members. *Cell* **2006**, *125*, 691−702. (b) Hillringhaus, L.; Yue, W. W.; Rose, N. R.; Ng, S. S.; Gileadi, C.; Loenarz, C.; Bello, S. H.; Bray, J. E.; Schofield, C. J.; Oppermann, U. Structural and evolutionary basis for the dual substrate selectivity of human KDM4 histone demethylase family. *J. Biol. Chem.* **2011**, *286*, 41616−25.
(26) Whetstine, J. R.; Nottke, A.; Lan, F.; Huarte, M.; Smolikov, S.; Chen, Z.; Spooner, E.; Li, E.; Zhang, G.; Colaiacovo, M.; Shi, Y. Reversal of histone lysine trimethylation by the JMJD2 family of histone demethylases. *Cell* **2006**, *125*, 467−81.
(27) Couture, J. F.; Collazo, E.; Ortiz-Tello, P. A.; Brunzelle, J. S.; Trievel, R. C. Specificity and mechanism of JMJD2A, a trimethyllysine-specific histone demethylase. *Nat. Struct. Mol. Biol.* **2007**, *14*, 689−95.
(28) Winters, D. K.; Cederbaum, A. I. Oxidation of glycerol to formaldehyde by rat liver microsomes. Effects of cytochrome P-450 inducing agents. *Biochem. Pharmacol.* **1990**, *39*, 697−705.
(29) Rose, N. R.; Ng, S. S.; Mecinovic, J.; Lienard, B. M.; Bello, S. H.; Sun, Z.; McDonough, M. A.; Oppermann, U.; Schofield, C. J. Inhibitor scaffolds for 2-oxoglutarate-dependent histone lysine demethylases. *J. Med. Chem.* **2008**, *51*, 7053−6.
(30) (a) Grasso, C. S.; Wu, Y.-M.; Robinson, D. R.; Cao, X.; Dhanasekaran, S. M.; Khan, A. P.; Quist, M. J.; Jing, X.; Lonigro, R. J.; Brenner, J. C.; Asangani, I. A.; Ateeq, B.; Chun, S. Y.; Siddiqui, J.; Sam, L.; Anstett, M.; Mehra, R.; Prensner, J. R.; Palanisamy, N.; Ryslik, G. A.; Vandin, F.; Raphael, B. J.; Kunju, L. P.; Rhodes, D. R.; Pienta, K. J.; Chinnaiyan, A. M.; Tomlins, S. A. The mutational landscape of lethal castration-resistant prostate cancer. *Nature* **2012**, *487*, 239−43. (b) Lapointe, J.; Li, C.; Higgins, J. P.; van de Rijn, M.; Bair, E.; Montgomery, K.; Ferrari, M.; Egevad, L.; Rayford, W.; Bergerheim, U.; Ekman, P.; DeMarzo, A. M.; Tibshirani, R.; Botstein, D.; Brown, P. O.; Brooks, J. D.; Pollack, J. R. Gene expression profiling identifies clinically relevant subtypes of prostate cancer. *Proc. Natl. Acad. Sci. U.S.A.* **2004**, *101*, 811−6.
(31) Hsu, K. C.; Cheng, W. C.; Chen, Y. F.; Wang, H. J.; Li, L. T.; Wang, W. C.; Yang, J. M. Core site-moiety maps reveal inhibitors and binding mechanisms of orthologous proteins by screening compound libraries. *PLoS One* **2012**, *7*, e32142.
(32) Black, J. C.; Manning, A. L.; Van Rechem, C.; Kim, J.; Ladd, B.; Cho, J.; Pineda, C. M.; Murphy, N.; Daniels, D. L.; Montagna, C.; Lewis, P. W.; Glass, K.; Allis, C. D.; Dyson, N. J.; Getz, G.; Whetstine, J. R. KDM4A lysine demethylase induces site-specific copy gain and rereplication of regions amplified in tumors. *Cell* **2013**, *154*, 541−55.
(33) Rose, N. R.; McDonough, M. A.; King, O. N.; Kawamura, A.; Schofield, C. J. Inhibition of 2-oxoglutarate dependent oxygenases. *Chem. Soc. Rev.* **2011**, *40*, 4364−97.
(34) Wang, L.; Chang, J.; Varghese, D.; Dellinger, M.; Kumar, S.; Best, A. M.; Ruiz, J.; Bruick, R.; Pena-Llopis, S.; Xu, J.; Babinski, D. J.; Frantz, D. E.; Brekken, R. A.; Quinn, A. M.; Simeonov, A.; Easmon, J.; Martinez, E. D. A small molecule modulates Jumonji histone demethylase activity and selectively inhibits cancer growth. *Nat. Commun.* **2013**, *4*, 2035.